



Weld defect localization in friction stir welding process

Debasish Mishra¹ · Sristi Shree³ · Abhinav Gupta⁴ · Ashok Priyadarshi⁵ · Sarthak M. Das⁶ · Surjya K. Pal⁷  · Debashish Chakravarty⁸ · Srikanta Pal⁴ · Tanushyam Chattopadhyay² · Arpan Pal²

Received: 4 October 2019 / Accepted: 6 November 2020 / Published online: 18 November 2020
© International Institute of Welding 2020

Abstract

The article attempts to detect the defects in friction stir welding (FSW) process by analyzing the signal acquired during welding. The said welding technique utilizes pressure and heat developed by the usage of a non-consumable tool. Thus, the axial force signal carries a lot of information about the physical process, and hence, it could be used to identify the weld defects. Signal analysis has been performed by using wavelet-based techniques. Before this analysis, a methodology has been followed to select the best mother wavelets suitable for the signal. The results of defect identification have been validated by mapping the processed signal with the actual weld quality.

Keywords Mother wavelet selection · Friction stir welding · Force signals · Defect identification

1 Introduction

The manufacturing sector has experienced a paradigm shift owing to globalization. They are now expected to cater to customer demands, i.e., being flexible about the varying product features each day. Demand for high precision products is on the rise as the traditional manufacturing style is getting obsolete. Integrating advanced manufacturing systems like sensory systems will help in achieving improved product quality at a low cost. Sensory systems integrated with mechanical components have been able to create a revolution in the manufacturing sector [1]. The manufacturing industries are under great thrust to reduce the cost of production, reduce the equipment downtime, and maintain the product quality.

As such, several advanced and innovative manufacturing methods are being adopted which are economically more effective and are environment friendly too. Friction stir welding (FSW) is one such manufacturing technique, and the details of the same have been discussed in the following paragraph.

The principle of FSW is indicated by its title which reads friction and stirring [2, 3]. For the friction, a tool with a specific design is utilized, which plunges inside the base materials to be joined, and generates the frictional heat (schematic of the process depicted in Fig. 1). Thus, the material for the tool (schematically depicted in Fig. 2) is selected based on the base materials to be welded. Upon plunging, the base materials get plastically deformed and attain flowability [3]. The stirring action is then achieved via a combined action of rotating the

Recommended for publication by Commission V - NDT and Quality Assurance of Welded Products

✉ Surjya K. Pal
skpal@mech.iitkgp.ac.in

¹ Advanced Technology Development Centre, Indian Institute of Technology Kharagpur, Kharagpur, India

² TCS Research and Innovation, Tata Consultancy Services, Kolkata, India

³ Department of Computer Science and Engineering, Birla Institute of Technology Mesra, Mesra, India

⁴ Department of Electronics and Communication Engineering, Birla Institute of Technology Mesra, Mesra, India

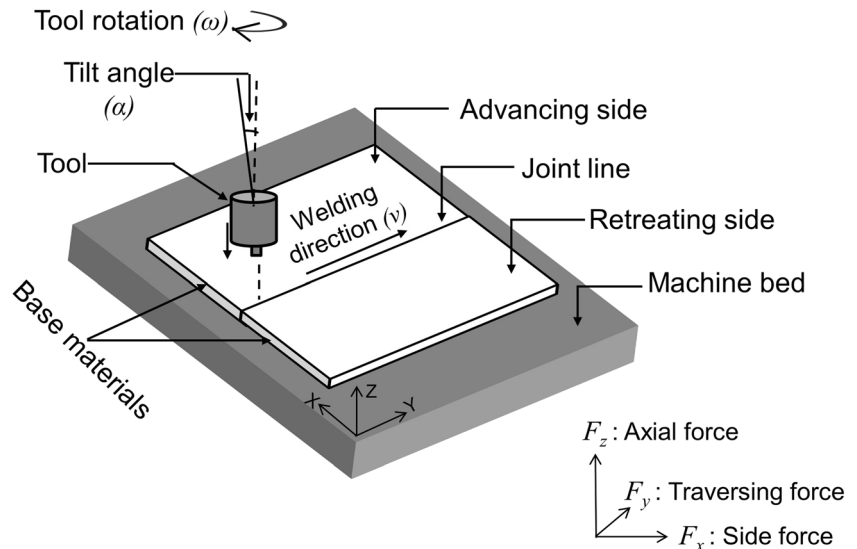
⁵ Mathematics and Computing, Birla Institute of Technology Mesra, Mesra, India

⁶ Information Technology, Birla Institute of Technology Mesra, Mesra, India

⁷ Department of Mechanical Engineering, Indian Institute of Technology Kharagpur, Kharagpur, West Bengal, India

⁸ Department of Mining Engineering, Indian Institute of Technology Kharagpur, Kharagpur, India

Fig. 1 Schematic diagram of the FSW process for a butt joint configuration



tool and translation of the machine's bed [4, 5]. This makes the deformed material stir alongside the edges of the tool, finally, forming the weld joint. FSW is being practiced in manufacturing sectors such as aerospace, automobile, railways, shipbuilding, and electronics [6–8]. The process has got numerous merits because of its occurrence in the solid state [9].

Out of the two base materials shown in Fig. 1, one of them is referred to as the advancing side. It is the one where the rotation vector's direction is the same as that of the welding direction [4]. The other has these vectors in opposite directions and is referred to as the retreating side [4]. The quality of welding is governed by parameters namely welding speed (v), rotational speed (ω), tilt angle (α), and plunge depth (p) [4, 9]. These are referred to as “joining parameters.” Other than these parameters, the weld quality is also affected by the dimensions of shoulder and pin which are categorized as “design parameters,” and the combination of base materials and tool material

under the category of “material parameters” [4, 9]. However, the former set of parameters can be controlled online while the latter is offline controllable [9].

The present work aims at the identification of weld defects; thus, it is imperative to discuss the typical weld defects encountered in the FSW process. With the aforementioned three categories of parameters in FSW, the associated weld defects can be classified into three namely, defects related to *excessive heating*, defects related to *insufficient heating*, and defect related to *design flaws* [9]. The *excessive heating* condition occurs with a higher value of ω , α , and p , and a lesser value of v , which deforms the base materials to be welded to a larger extent resulting in melting [10]. This makes the shoulder of the tool incapable to uphold the material within its surface, leading to material loss, which is referred to as *nugget collapse*. As a result, a chunk of the lost material gets accumulated alongside the boundary of the welded zone which is referred to as a *flash*, and the remaining probably gets stuck to the tool, being referred as *surface galling* [11]. Also, because of the high heat availability, another defect named *sticking* occurs, where the bottom part of the plates to be welded gets stuck to the machine bed. The second category, i.e., the *insufficient heating* condition occurs with lower values of ω and higher values of v . In this condition, the parametric combination fails to deform the materials plastically. The defects which arise in such a situation are discussed in the following sentences. A *wormhole* or *tunnel* is one of the defects under this category, which occurs because of material loss [5]. It is also referred to as volumetric defects [12]. This defect may occur because of the high values of v which reduces the contact time between the tool and the base materials [10]. This thereby fails to deform the materials to be welded, and as such, the tool interacts with material which almost is in its ambient condition. This interaction, instead of stirring the materials, results in the formation of *voids* and *pits* in the weld zone.

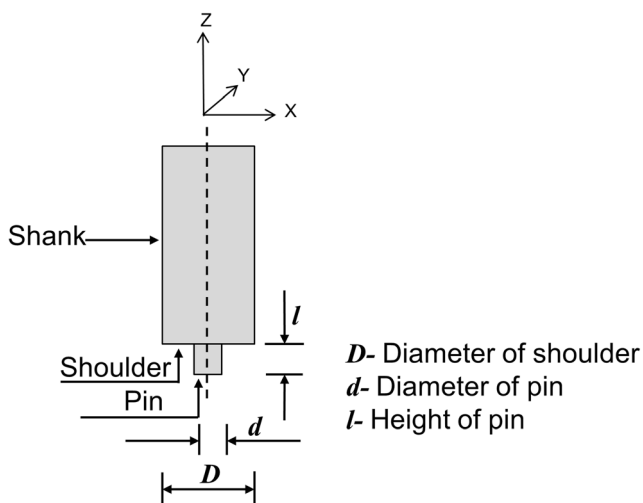


Fig. 2 Schematic diagram of the FSW tool

Another defect is the *lack of fill* which occurs with an insufficient value of p during welding [13]. *Kissing bond* is the name given to a defect that occurs because of improper fusion of the materials, i.e., the weld joint lacks a metallurgical bonding [14]. Other defects encountered are *overpenetration* and *lack of penetration* which are related to the flaws in design [2]. If the height of the pin (l) is equal to or more than the thickness of the base materials, it probably may hit the machine bed surface, destroy the tool, and will result in defects. This is referred to as *overpenetration*. On the other hand, a lesser value of l as compared to the base materials' thickness will fail to obtain a fully consolidated weld joint, resulting in a *lack of penetration*. The literature suggests the pin height to be lesser than the thickness of the base materials by 0.2 to 0.3 mm [2].

Fabrication is essential to industries and is expensive as well. The structure/part obtained after fabrication is subjected to several tests to ensure the quality and durability of the welded joint. These tests may be destructive and non-destructive. Both these means involve expenditure and time. Instead, the defects in a weld can be determined by monitoring a few physical parameters which are relevant to the FSW process. These include force, torque, acoustic emission (AE), power signals, etc. which are imperative to the FSW process [9]. As the present work aims at the identification of defects by monitoring the physical parameters, the following paragraph discusses the literature reported on the automation of the FSW process. This section appreciates the individual works which have been reported by other researchers mentioning its importance and concurrently reports the lack of the work as well.

Researchers have attempted to monitor FSW by acquiring various signals such as force, torque, and AE [15–18]. The force and torque signals have been utilized for defect identification. The signal analysis includes the application of *discrete wavelet transform* (DWT) where the *Daubechies* family ($db4$) has been utilized as the mother wavelet [15]. The detail coefficients of the two signals up to three levels were extracted and the square of errors of the detail coefficients was utilized as a feature for identification of the faults. A higher amplitude of the selected feature was found for the regions of the weld with defects. A good correlation can be observed between the defects in the welded sample and the extracted feature from the signal. However, the justification for the use of $db4$ for the analysis has not been reported. A similar investigation for the identification of defects has also been carried out by applying *continuous wavelet transform* (CWT) on the force signals by using $db8$ as the mother wavelet [16]. In this study, the variance of the signal has been extracted as a feature. A higher intensity of the extracted feature was observed for the defective weld region as compared to the defect-free regions of the weld. Though a new technique for defect identification in FSW has been reported through this work, the CWT technique requires more computation time as compared to DWT, which

limits the usage of CWT in real-time applications. Moreover, this work also does not justify the use of $db8$ as the mother wavelet. The force signal and power consumption by the machine over the welding period have been utilized in another study for differentiating the defective and defect-free welds in the FSW process [19]. The said signals have been analyzed via DWT, where the detailed coefficients have been extracted up to six levels. A study on optimization has also been reported for the selection of level of decomposition. Out of the two, the power signal has been found to provide more information as compared to the force signal. The reason reported in the paper is the external connection of the power sensor which does not get affected by the components of the FSW machine, whereas the force sensor was inbuilt to the machine. One more probable reason to this could be the inherent availability of the power signal in the system. During the welding process, with the occurrence of any abnormality, the current and voltage consumption in the motors will vary. Thus, this will get reflected in the power consumed over time. However, the article does not discuss about the mother wavelet which is essential information in the process of DWT for analysis of any signal.

Other than the force signal, the AE signal has been acquired to monitor the FSW process. One such work reports about the monitoring of *gap* defects [17]. This defect occurs when there is a gap in the abutting edges of the two base materials to be welded. Since FSW relies on frictional heat and mechanical deformation of the base materials, it is important to ensure that the materials fixed on the fixture of the machine are alongside each other, which will be one of the primary factors for obtaining a consolidated joint. This principle of FSW is also the reason for the utilization of AE signal which is generated in metals undergoing plastic deformation. Thus, the AE signals are inherently generated during the welding. The signals were processed via DWT by using $db6$ as the mother wavelet, and the energy of the wavelet coefficients was extracted as a feature for the identification of those defects. Though the differentiation between a normal and defective weld has been successfully shown, the AE signal acquisition was carried out at a sampling rate of 1 MHz, which is significantly high for real-time applications. Furthermore, the information regarding the suitability of the utilized mother wavelet is also lacking. The *gap* defects have also been monitored by acquiring force signal where a drop in the signal was found whenever the tool approached the gap in the abutting edges of the weld [20]. Though the drop in the force signal corresponds to approximately 1000 N for a gap of 0.05 mm, a negligible drop has been reported for smaller gaps.

Furthermore, to classify the welds into defective and defect free, DWT has been applied to the weld images where *coiflet* has been utilized as the mother wavelet for decomposing the images [21]. Features extracted from the approximation coefficients were variance, energy, and entropy. The range of

energy for the defect-free weld has been reported to be in the range of 99.74 to 99.93 and that of in the range of 99.21 to 99.51 for the defective welds. Similarly, the variance and entropy features of the approximation coefficients have clear separation for defect-free and defective welds. These features were then utilized to train a support vector machine model for classifying the welds. One limitation of this work is the use of the image for quality analysis which could only provide the information present on the weld surface and overlooks the presence of internal defects which rather is also necessary. Furthermore, no information has been reported as to why the *coiflet* is used in the analysis.

Other reported studies are concerned with the effect of varying process parameters (ω , v , and p) in FSW [18]. The AE signal was acquired for this study and was analyzed in the time domain, and other techniques such as DWT and *fast Fourier transform* (FFT). The time-domain AE signal is found to be an indicator of the fluctuations in the values of p , where it has been observed that with insufficient contact between the tool and the workpiece, the amplitude of the signal was highly random. This randomness stabilized with proper contact between the two. This also suggests the importance of the AE signal which could be utilized to ensure proper contact between the tool and the workpiece during welding. With DWT, the approximation plot has been found providing information about the proper contact between the tool and the workpiece. However, as mentioned earlier for the AE signal, the sampling rate involved is very high which limits its usage in real-time applications. Furthermore, the study has not reported the mother wavelet used for performing DWT. Another study attempts to monitor the change in tool pin profiles by applying DWT on vibroacoustical signals acquired during the welding [22]. Two different pin profiles, one with groove and the other with flutes, were selected, and the signals acquired during fabrication with these two tools have been classified. The signals were analyzed by using *db5* as the mother wavelet. Three features namely, root mean square (RMS), variance, and median were extracted from the approximation coefficients of the decomposed signals. Out of the three features, the median outperformed the other two features in classifying the tools. In addition to this analysis, the approach may be utilized in studying whether, with the wear of the tool, any information can be gathered from the signal. But again, it must also be noted that the vibroacoustical signals need a high sampling rate. This will lead to the generation and processing of a huge amount of data which would require devices with high processing power and space. This would limit its usage for real-time applications. Furthermore, in the context of signal analysis, the suitability of *db5* has not been reported. A comprehensive review of the research works on the automation of FSW can be referred from the cited literature [9, 23].

From the aforementioned literature, it can be inferred that the potential of the *wavelet transform* is massive in identifying

the faults from the transient signals. Signal processing, proper analysis, and extraction of the information are crucial for manufacturing operations to keep a track of the process and eradicate wastage of resources. The signals acquired from manufacturing operations mostly consist of transient events [9]. Thus, processing them via the time-domain methods will be insufficient because the said technique will not report the frequencies present in the signal. The *Fourier transform* technique can be applied to find the frequency components. However, upon transforming, the time information is lost, and they are effective for stationary signals [19]. For identification of the frequencies present in a signal with the time information, time-frequency analysis is needed. Thus, proper and precise identification of faults in the process can be achieved by processing the signals through *wavelet transform* [15, 16]. The *wavelet transform* however depends upon the selected mother wavelet, and from the literature reported, it can be observed that the art of the same is lacking for FSW. For investigation on this, the axial force signal has been considered. A methodology for identification of the best mother wavelet has been identified and presented. The test for the same has been investigated via 42 different welded samples. This has been followed by the presentation of another technique for identification and localization of the weld defects by analyzing the axial force signal through DWT with the best mother wavelet. The following section discusses the methodology followed in the study.

2 Methodology

The welding process gives rise to three forces namely: axial force (F_z), traversing force (F_y), and side force (F_x), as shown in Fig. 1. The F_z acts vertically and it arises as a result of the tool trying to maintain a desired position during the welding. The F_y acts parallel to the motion of the tool, which is a result of the opposition of the material to the motion of the tool. Finally, the F_x acts perpendicular to the traverse direction. The welds are achieved through the pressure and the frictional heat. At any point, if the contact between the tool and base materials is disturbed, or the pressure that has to be exerted by this tool lowers down, then it would result in defective welds. Thus, the signature of F_z is of higher importance than that of F_y and F_x . The present work thus makes use of the F_z signal for defect identification and localization.

In the present work, a computer numerically controlled (CNC) FSW machine is selected, which has an inbuilt load cell to acquire the F_z signal. The first objective was to understand the behavior of this signal. F_z is a non-stationary signal, i.e., it is transient. A signal is considered transient if it contains transient events, which are described as an abrupt change in phase, frequency, or amplitude of the signal. Considering an abrupt change in the amplitude in the case of a transient event,

a large RMS value of a window applied on the signal will indicate the probability of the existence of transient events. A simple method for identifying these probable transients is to consider those RMS values which are crossing a certain threshold for a given signal.

Figure 3 depicts the variation of an F_z signal during the welding phase, and the same corresponds to a defective weld. It can be said defective in a sense that the parameters utilized to fabricate the weld were so chosen that a defective weld was obvious. Severe fluctuations can be seen in the amplitudes, which were because of the change in the process parameters (ω and ν) during welding. To calculate the threshold, various non-adaptive thresholding methods can be applied to a signal namely, *Donoho's universal method* and *statistics-based threshold* [24]. The mathematical equations for the two techniques are depicted in Eqs. (1), (2), (3), and (4), respectively [24].

$$T_D = \sigma \times \left(\sqrt{2(\log(n))} \right) \tag{1}$$

$$\sigma = \frac{\text{Median}(|W_{j,k}|)}{0.6745} \tag{2}$$

$$T_{S1} = \text{Mean}(S) + 2 \times \text{Std.}(S) \tag{3}$$

$$T_{S2} = 1.5 \times \text{Std.}(S) \tag{4}$$

In the above equations, σ is the estimation of the average variance of the noise, n is the length of the signal, $W_{j,k}$ represents all the wavelet coefficients at scale 1 of the signal with j being the scale parameter and k represents the shift parameter, S represents the original signal, T_D stands for the threshold calculated by *Donoho's method*, and T_{S1} and T_{S2} stand for the threshold calculated using the *statistical-based method*.

Figure 4 represents the plot of RMS values of the original signal depicted in Fig. 3 calculated over a window of 10. The threshold values (T_D , T_{S1} , and T_{S2}) are depicted in the same

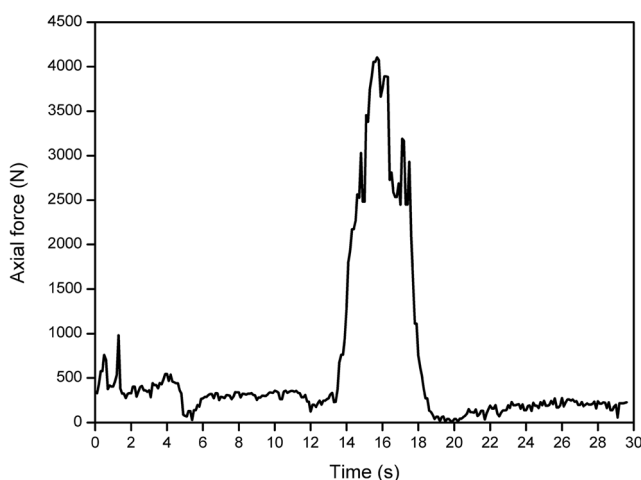


Fig. 3 Plot of the original signal showing the variation of axial force with time

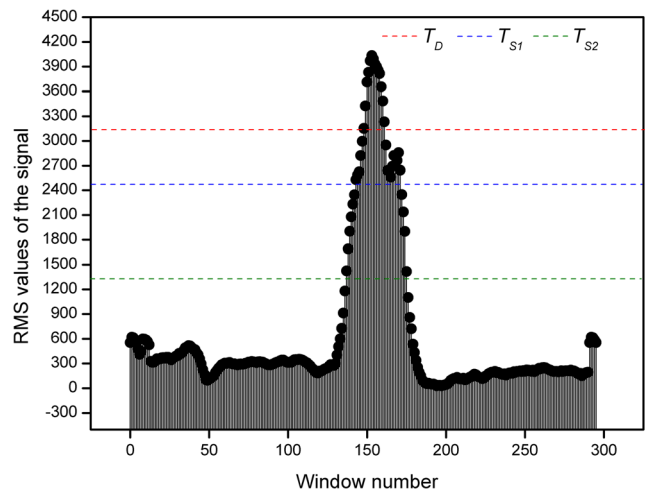


Fig. 4 RMS values and thresholds plot

plot. The RMS values can be seen to be crossing these thresholds which are indications of abrupt changes in the amplitude of the signal and thus, they represent a high probability of occurrence of transient events. Similarly, the transient characteristic of a signal in the time-frequency domain is characterized by an abrupt change in the frequency, phase, and the amplitude of the signal. This can be validated by calculating the RMS values of the 1st-level detail coefficients of the original signal. By using the thresholding schemes discussed above, an abrupt change in frequency and amplitude can be identified by looking at the RMS values crossing the threshold, indicating a high probability of the existence of a transient event. Figure 5 is the representation of this discussion.

Owing to the transient characteristics of the F_z signal, processing of the same in the time domain or frequency domain may not yield significant results. Instead, a time-frequency-based approach such as wavelets will be best suited for the transient signals which will provide information about both time and frequency. This is more relevant to the

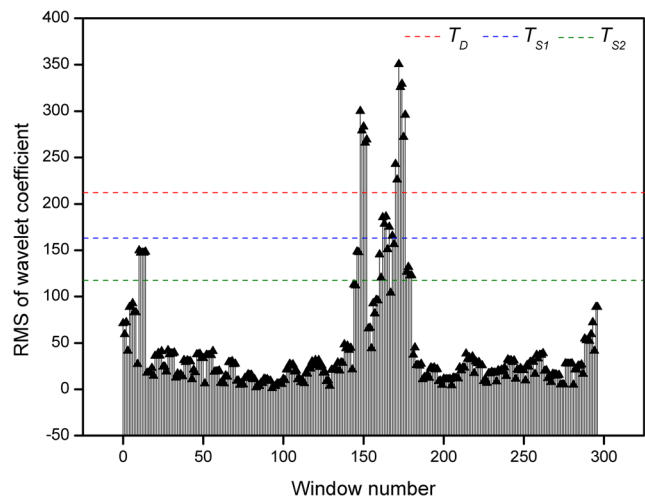


Fig. 5 RMS values of the 1st-level wavelet coefficients and thresholds plot

manufacturing processes. After studying the signal, the next objective was to come up with a technique for the selection of a mother wavelet, which is discussed in the following paragraph.

Wavelets can be defined as waves that exist for a limited duration of time, have an irregular shape, and a zero mean value [25, 26]. Mother wavelets are the basis vectors in the case of the *wavelet transform* [27]. DWT decomposes a signal into different frequency bands [28, 29]. The signal upon decomposition yields wavelet coefficients namely, detail and approximation. By nature, the detail coefficients are sparse, which is the primary reason for its huge range of applications in the field of compressive sensing. Recent studies in FSW have utilized the wavelet coefficients extracted by DWT for real-time monitoring and control of the process and monitoring of the tool quality [1, 30]. In this process, it is crucial to choose a suitable mother wavelet for a particular signal as different mother wavelets may produce different results.

Wavelets exist as families which can be categorized into two namely, orthogonal and biorthogonal. Orthogonal wavelet family members offer a perfect reconstruction of the signals, are concise, and are computationally inexpensive [31]. In the present work, 32 orthogonal wavelets have been selected which include (a) *db2 to db15* (from *Daubechies* family), (b) *sym2 to sym15* (from *Symlet* family), (c) *coif2 to coif5* (from *Coiflet* family), and 14 biorthogonal wavelets which include (d) *bior1.1, bior1.3, bior1.5, bior2.2, bior2.4, bior2.6, bior2.8, bior3.1, bior3.3, bior3.5, bior3.7, bior4.4, bior5.5, and bior6.8*. The *db1* of the *Daubechies* family is the simplest wavelet and is called the *Haar* wavelet, and the same has not been included in the study because of its low vanishing moment. Similarly, *sym1* and *coif1* have also been excluded from the analysis [32]. The biorthogonal wavelet is a new extension to the wavelet family. It uses one mother wavelet for decomposition and another for synthesis. The analysis has been carried out in two different forms: (a) considering only the orthogonal family and (b) considering both orthogonal and biorthogonal families. Such a classification has been followed because the biorthogonal family is computationally expensive and takes more time [31]. The decomposition has been carried out for each signal up to the first level because features extracted from subsequent levels are not being able to localize properly with the defects present in the signal.

As DWT provides the wavelet coefficients by analyzing the signal, the higher the magnitude of the wavelet coefficients, the higher will be the correlation between the analyzed signal and the mother wavelet used for analysis. High magnitudes correspond to high energy [33]. The energy content is given as the sum of squares of magnitudes of coefficients at a scale and has been depicted in Eq. (5). At the same time, it is also crucial to minimize entropy which indicates the disorder in the frequency response and quantifies the distribution of energy at different scales of decomposition. The mathematical

equation for the entropy measure has been depicted in Eq. (6). The performance of a mother wavelet can be judged by these two parameters, i.e., it must yield maximum energy while producing minimum entropy. Combining these two parameters, the new parameter defined is known as energy to Shannon entropy ratio which will serve as the basis for the determination of a suitable mother wavelet for a signal [34]. The base wavelet should give maximum energy to the entropy ratio. This is also known as the maximum energy to Shannon entropy ratio criterion.

$$\text{Energy}(j) = \sum_{k=1}^K |w(j, k)|^2 \quad (5)$$

$$S_{\text{entropy}}(j) = - \sum_{k=1}^K p_k \log_2 p_k \quad (6)$$

$$p_k = \frac{|w(j, k)|^2}{\text{Energy}(j)} \quad (7)$$

$$\text{Ratio}(j) = \frac{\text{Energy}(j)}{S_{\text{entropy}}(j)} \quad (8)$$

where p_k refers to the energy probability distribution of the wavelet coefficients.

The performance of a selected wavelet needs to be evaluated for a given signal to check whether the criteria selected has any improvement in the amount of information extracted from the raw signal [35, 36]. A significant fluctuation in the detail coefficients is observed during the occurrence of a defect. This fluctuation is used in the identification of defective weld regions. But the detail coefficients alone cannot distinguish between the defective region and defect-free regions. This is because the rise in magnitudes may also result in false positives for the occurrence of a defect, and there are no threshold selection criteria to separate the detail coefficients of defective regions from those of defect-free regions. Therefore, some other statistical parameter is needed for identifying the defective region and to show which mother wavelet can do that by extracting the maximum amount of information about the defect from the raw signal. According to the available literature [15, 19], the square of errors has been used as a metric to identify defects which necessarily indicates the variance of data points. As pointed in another literature [34], the *kurtosis* of the detail coefficients obtained by applying DWT on a signal represents the presence of outliers better than the variance and at the same time, it also eliminates the transient noise in the signal, if any. *Kurtosis* is an established method for studying the shape characteristics of a signal. It is fundamentally independent of the signal-to-noise ratio of the data; thus, the same criterion can be applied to the entire dataset, which is an additional advantage over the use of variance. Therefore, in this study, *kurtosis* of the DWT is considered for defect identification. The mathematical equation for

determining *kurtosis* has been depicted in Eq. (9).

$$k = \frac{n(n+1)(n-1)}{(n-2)(n-3)} \frac{\sum_{i=1}^n (X_i - \bar{X})^4}{\left(\sum_{i=1}^n (X_i - \bar{X})^2\right)^2} \tag{9}$$

where *n* is the length of the signal, *X_i* is the *i*th data point of the signal being considered, \bar{X} represents the mean of the signal, and *k* stands for *kurtosis*.

Since *kurtosis* will return a single value for a given signal, therefore, to map the defective regions with the values of the *kurtosis*, the same has been evaluated on windows of 100 samples. The selected window size is based on observations whose evaluation begun with a window size of 10 samples and finally reached a value providing optimal results for a defective region in a welded sample. The *kurtosis* plots of various mother wavelet families are observed and the wavelet depicting the presence of a defect in the sample is verified with the selection criteria presented and finally selected for defect identification by using force sensor signal. The next section mentions the experiments that have been carried out in this study.

3 Experiments

This section provides the details about the experiments related to the fabrication of the welds through FSW and the process of signal acquisition during the welding.

FSW was performed on two aluminum sheets (AA6061) welded in butt joint configuration. The FSW machine is having a capacity of 2 ton (WS004, ETA Technology), and it

Table 1 Tool dimensions

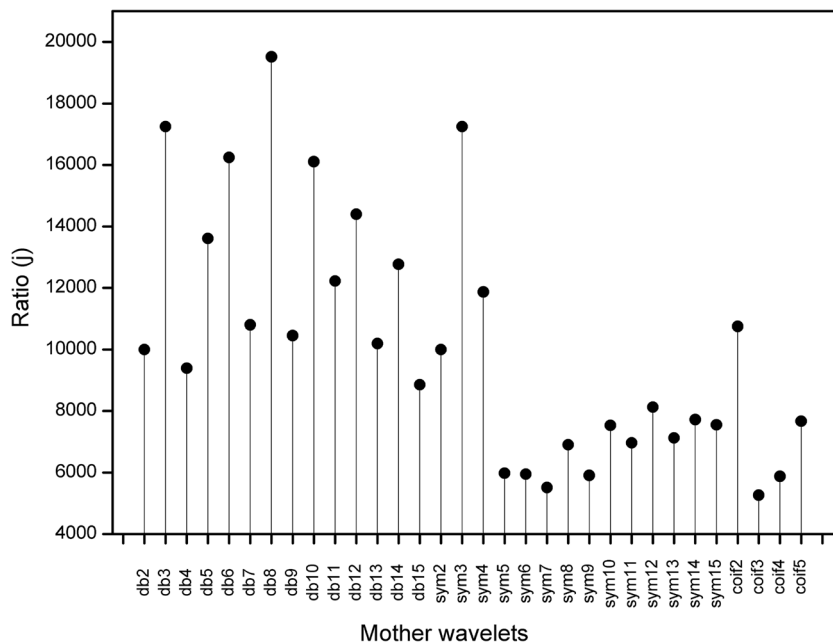
Shoulder diameter (in mm)	18
Pin diameter (in mm)	6
Pin length (in mm)	2.6

works on a displacement mode. The tool utilized was machined from the H13 tool steel material and the dimensions of this tool have been given in Table 1. The equipped load cell captures the force signature during welding. The machine is also equipped with LABVIEW for the acquisition of the captured data at a sampling rate of 10 Hz. After the welding, the acquired signals were transferred to a local computer which was then processed through MATLAB for selection of mother wavelet and feature extraction. The feature map was then studied for identifying the weld defects. To validate the results obtained by analyzing the acquired signals, the fabricated welds were scanned via a 3D X-ray micro-computed tomography (CT) system (Phoenix vtome x s, General Electric) to find the internal defects in those welds.

4 Results and discussion

To begin with the presented methodology for finding the best mother wavelet, several welds were fabricated considering AA6061 material. Nearly 42 welds were fabricated with six different values of ω and seven different values of ν . These 42 welds were ranked based on their ultimate tensile strength. The force signal of the best weld sample ($\omega = 1000$ rpm and ν of 200 mm/min) out of the 42 welded samples was analyzed with the proposed methodology for the selection of the best

Fig. 6 Plot of energy to entropy ratio values corresponding to selected mother wavelets (orthogonal family) for a welded sample



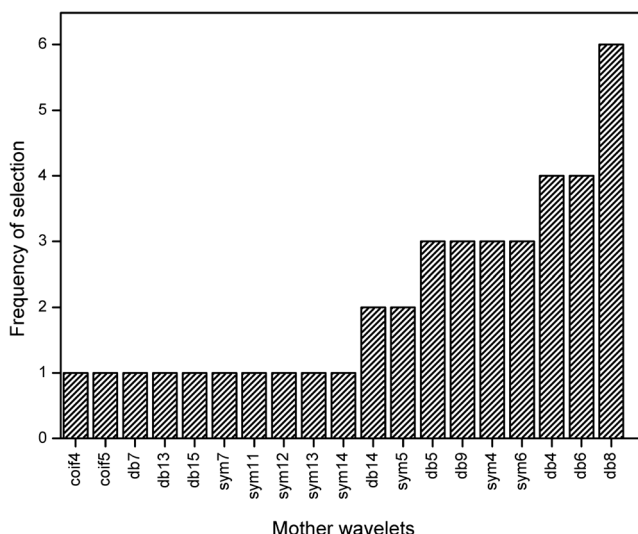


Fig. 7 Histogram plot for selection of orthogonal mother wavelets

mother wavelet. For the analysis, only orthogonal mother wavelets have been considered, and the result of the same has been depicted in Fig. 6.

From Fig. 6, it can be seen that the highest ratio is obtained for *db8* for the said welded sample. Thus, *db8* is chosen as the most appropriate mother wavelet for this sample. Similarly, the best mother wavelets were determined for the remaining 41 welded samples, and the histogram plot depicting the counts of the same has been depicted in Fig. 7. Results indicate that *db8* is the most selected mother wavelet in the entire selected list. Other than *db8*, *db6* and *db4* can also be found to have a higher ratio.

For the validation of the obtained mother wavelets, the correlation between features extracted through *kurtosis* has been mapped with the defects present in the different weld samples. As mentioned in the preceding section, two welded samples have been chosen for this purpose with internal defects. The results of those welded samples have been shown in the following sections.

4.1 Orthogonal wavelets

Figure 8 shows the physical weld image of a welded sample (parameters: ω of 500 rpm and v of 40 mm/min). The corresponding force signal has been decomposed via DWT by using *db8* as the mother wavelet. The fluctuations of the *kurtosis* values obtained for the signal analyzed via *db8*, along with the corresponding CT scan image have been depicted in Fig. 9. The extracted feature has a high magnitude wherever a defect is present in the welded sample.

Fig. 8 Picture of the welded sample

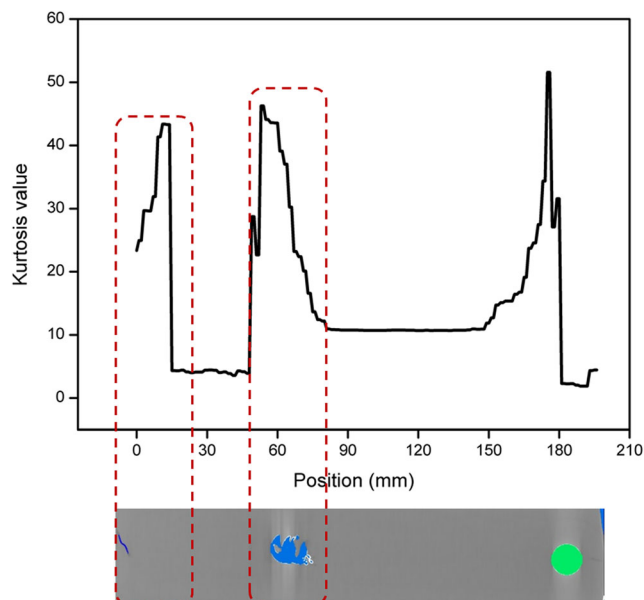


Fig. 9 Plot of *kurtosis* values of the 1st level detail coefficients of force signal with *db8* mother wavelet versus X-position and corresponding CT scan image

The peaks in the plots mostly correspond to the weld defects present in the welded sample. The peak in the *kurtosis* map at the start of the weld is because of the start in the movement of the tool which resembles the start of the welding phase. Before this phase, the tool was in the plunging position and dwelling at the same location. Then, the machine bed starts moving and the weld joint is fabricated. The peak at the end of the *kurtosis* map corresponds to a hole in the CT scan image which is referred to as the keyhole in FSW caused by the removal of the tool from the welded sample. Some other low magnitude peaks in the plot can be accounted for the noise and vibrations caused by the machine since the force sensor is integrated with the machine itself.

Referring to Fig. 7, the four other mother wavelets which are performing good apart from *db8* are *db6*, *db4*, *sym6*, and *sym4*. To make a comparative analysis among these five mother wavelets (i.e., *db8*, *db6*, *db4*, *sym6*, and *sym4*), the *kurtosis* values of all five of these mother wavelets considering the wavelet coefficients of the force signal have been depicted in Fig. 10. From the figure, it can be seen that the highest magnitude at locations where the defect is present is being obtained by using *db8*. The other wavelets (*db6*, *db4*, *sym6*, and *sym4*), though are being able to localize the defect positions, the rise in magnitude in defect regions is not enough in comparison to *db8*.

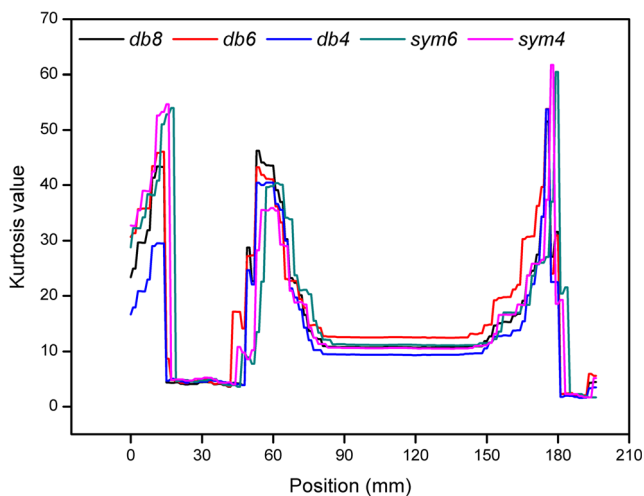


Fig. 10 Comparison of kurtosis values of the 1st-level detail coefficients of force signal with *db8*, *db6*, *db4*, *sym6*, and *sym4* mother wavelets versus X-position for the sample

Similarly, Fig. 11 shows the picture of another welded sample (parameters: ω of 2000 rpm and v of 40 mm/min). Figure 12 shows the corresponding extracted *kurtosis* values from the 1st-level detail coefficients of the force signal of the welded samples shown in Fig. 11. The detail coefficients have been extracted by using *db8* as the mother wavelet. Along with this figure, the corresponding CT scan image of the welded sample has also been shown to validate the results obtained. It can be seen that the extracted feature has a high magnitude wherever a defect is present in the welded sample. Furthermore, the comparison plot among the mother wavelets has been depicted in Fig. 13. From the figure, it can be seen that the highest magnitude at locations where the defect is present is being obtained by using *db8*. The other wavelets (*db6*, *db4*, *sym6*, and *sym4*), though are being able to localize the defect positions, the rise in magnitude in defect regions is not enough in comparison to *db8*.

4.2 Orthogonal and biorthogonal wavelets

This section compares the results obtained by *db8* (the best mother wavelet obtained in the preceding section) with the 14 selected mother wavelets of the biorthogonal family. Figure 14 shows the variation of energy to entropy ratio for the selected mother wavelets for a welded sample. It can be seen that the ratio is highest for the *bior5.5* wavelet. Thus, *bior5.5* may be chosen over *db8* as the most appropriate wavelet for this welded sample. Thus, selecting *bior5.5* as the mother wavelet instead of *db8* to analyze the force signal and extract the

Fig. 11 Picture of the welded sample

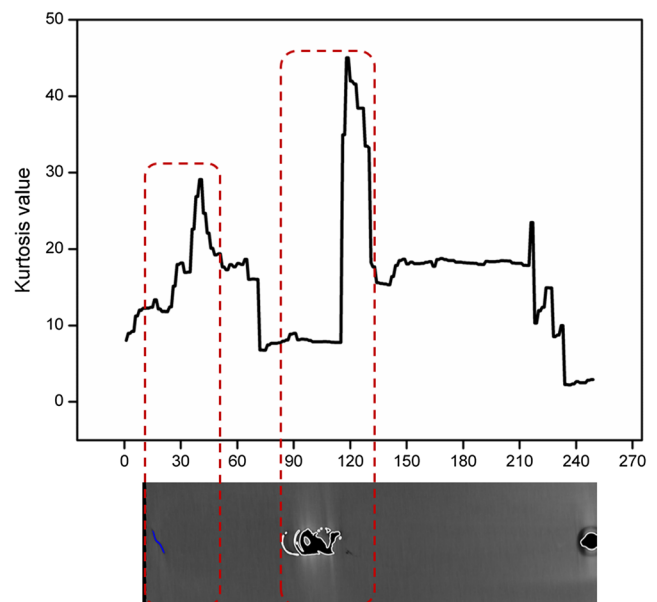
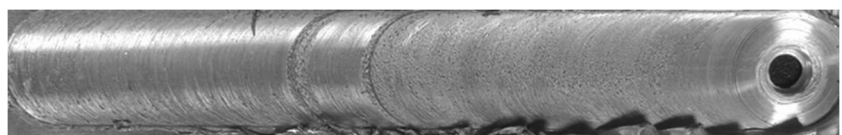


Fig. 12 Plot of *kurtosis* values of the 1st-level detail coefficients of force signal with *db8* mother wavelet versus X-position and corresponding CT scan image

selected feature, the defect localization may be more accurate. This is because of the higher energy to entropy ratio being possessed by this mother wavelet, which assures that it can extract more information from the signal as compared with other mother wavelets. However, the biorthogonal family has extra computational cost and time lag associated with it, whereas the orthogonal family is faster and computationally less expensive. This limits the usage of the biorthogonal family in real-time applications. Thus, *db8*, as obtained from the orthogonal family, can be preferred in real-time applications where computational resources are constrained.

As discussed earlier, F_y is the traversing force that acts parallel to the motion of the tool, and it arises as a result of the opposition of the material to the motion of the tool. F_x is the side force that is perpendicular to the traverse force. The weld formation in FSW is dependent upon a proper combination of the joining parameters, which would result in a good quality weld, as it governs the frictional heat availability needed for proper mixing of the material leading to the required strength of the weld. The frictional heat is coming from the plunging and rotating action of the tool. Thus, at any point, if the contact between the tool and the base materials is disturbed, i.e., if the contact is improper, then defects would be generated. A majority of the weld defects such as *wormhole* or *tunnel*, *voids*, and *surface cracks* can be identified by analyzing the F_z signal because this force arises as a result of the tool

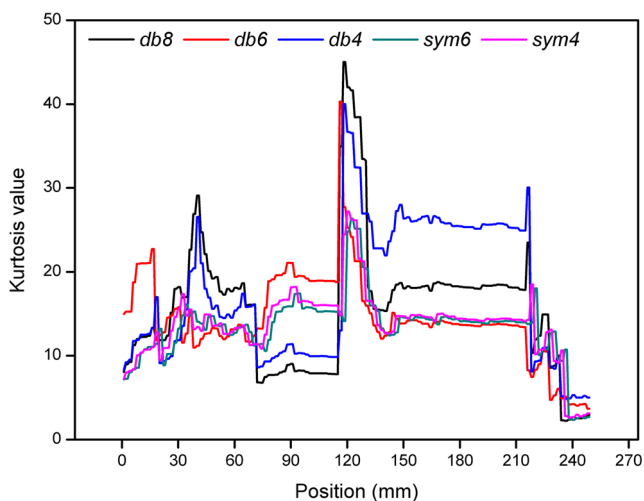


Fig. 13 Comparison of kurtosis values of the 1st-level detail coefficients of force signal with *db8*, *db6*, *db4*, *sym6*, and *sym4* mother wavelets versus X-position

trying to maintain a desired position during the welding. Thus, in this study, the F_z has been considered for the identification of a wide range of defects. F_y and F_x may prove better for identifying the defect such as *flash* which indicates the accumulation of the weld material alongside the edge of the weld zone or defect such as voids in the joint line. In the future, all three forces can be considered for defect identification.

5 Conclusion

DWT is used for the time-frequency domain analysis of the force sensor signal. The detail coefficients thus acquired can be used to identify the presence of defects introduced during welding. The use of different mother wavelets in DWT

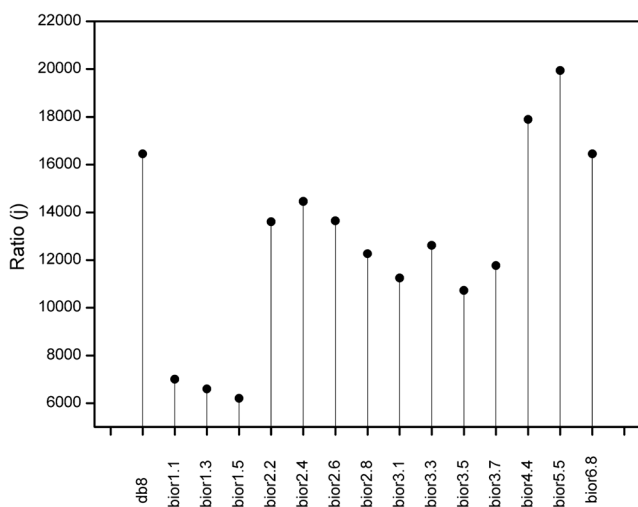


Fig. 14 Plot of energy to entropy ratio values corresponding to selected mother wavelets (*db8* from orthogonal family and selected biorthogonal family)

produces a different set of coefficients; therefore, the selection of an appropriate mother wavelet depicting the presence of a defect most accurately is of utter importance. With the use of a statistical tool, i.e., *kurtosis*, on the detail coefficients of the first-order decomposition, it was observed that the obtained values of *kurtosis* map accurately with the presence of defects in the welded samples. The strategy presented here can help industries practicing FSW to check the presence of weld defects in the welded sample. In the future, all three forces can be considered for defect identification and can also be utilized in building real-time control algorithms for the FSW process.

Funding This research is an outcome of the project funded by the Department of Heavy Industry of the Ministry of Heavy Industries & Public Enterprises, Government of India, and TATA Consultancy Services (Grant No: 12/4/2014 – HE&MT).

References

- Roy RB, Mishra D, Pal SK, Chakravarty T, Panda S, Chandra MG, Pal A, Misra P, Chakravarty D, Misra S (2020) Digital twin: current scenario and a case study on a manufacturing process. *Int J Adv Manuf Technol* 107:3691–3714. <https://doi.org/10.1007/s00170-020-05306-w>
- Thomas W, Nicholas E (1997) Friction stir welding for the transportation industries. *Mater Des* 18:269–273. [https://doi.org/10.1016/S0261-3069\(97\)00062-9](https://doi.org/10.1016/S0261-3069(97)00062-9)
- Mishra RS, Mahoney MW (2007) Friction stir welding and processing. *ASM Int* 368. <https://doi.org/10.1361/fswp2007p001>
- Jain R, et al. (2015) Friction Stir Welding: Scope and Recent Development. In: Davim J. (eds) *Modern Manufacturing Engineering. Materials Forming, Machining and Tribology*. Springer, Cham. https://doi.org/10.1007/978-3-319-20152-8_6
- Mishra D, Sahu SK, Mahto RP et al (2019) Friction stir welding for joining of polymers. Springer, Singapore, pp 123–162
- Ding J, Carter B, Lawless K, Nunes A, Russell C, Schneider J (2006) A Decade of Friction Stir Welding R and D at NASA's Marshall Space Flight Center and a Glance into the Future
- Fred Delany SWK, MJR (2007) Friction stir welding of aluminium ships. <http://www.twi-global.com/technical-knowledge/published-papers/friction-stir-welding-of-aluminium-ships-june-2007/>. Accessed 25 Sep 2019
- Davenport J, Kallee SW, Wylde JG (2015) Creating a stir in the rail industry. <http://www.twi-global.com/technical-knowledge/published-papers/creating-a-stir-in-the-rail-industry-november-2001/>. Accessed 25 sept 2019
- Mishra D, Roy RB, Dutta S, Pal SK, Chakravarty D (2018) A review on sensor based monitoring and control of friction stir welding process and a roadmap to Industry 4.0. *J Manuf Process* 36:373–397. <https://doi.org/10.1016/j.jmapro.2018.10.016>
- Podrzaj P, Jerman B, Klobcar D (2015) Welding defects at friction stir welding. *Metalurgija* 54:387–389
- Ahmadi H, Arab NBM, Ghasemi FA, Farsani RE (2012) Influence of pin profile on quality of friction stir lap welds in carbon fiber reinforced polypropylene composite. *Int J Mech Appl* 2:24–28. <https://doi.org/10.5923/j.mechanics.20120203.01>
- Zhao Y, Zhou L, Wang Q, Yan K, Zou J (2014) Defects and tensile properties of 6013 aluminum alloy T-joints by friction stir welding. *Mater Des* 57:146–155. <https://doi.org/10.1016/j.matdes.2013.12.021>

13. Rajiv Mishra, Partha Sarathi De, Nilesh Kuma, Friction Stir Welding and Processing, Springer International Publishing. <https://doi.org/10.1007/978-3-319-07043-8>
14. Li B, Shen Y, Hu W (2011) The study on defects in aluminum 2219-T6 thick butt friction stir welds with the application of multiple non-destructive testing methods. *Mater Des* 32:2073–2084. <https://doi.org/10.1016/j.matdes.2010.11.054>
15. Kumar U, Yadav I, Kumari S, Kumari K, Ranjan N, Kesharwani RK, Jain R, Kumar S, Pal S, Chakravarty D, Pal SK (2015) Defect identification in friction stir welding using discrete wavelet analysis. *Adv Eng Softw* 85:43–50. <https://doi.org/10.1016/j.advengsoft.2015.02.001>
16. Kumari S, Jain R, Kumar U, Yadav I, Ranjan N, Kumari K, Kesharwani RK, Kumar S, Pal S, Pal SK, Chakravarty D (2016) Defect identification in friction stir welding using continuous wavelet transform. *J Intell Manuf* 30:1–12. <https://doi.org/10.1007/s10845-016-1259-1>
17. Chen C, Kovacevic R, Jandgric D (2003) Wavelet transform analysis of acoustic emission in monitoring friction stir welding of 6061 aluminum. *Int J Mach Tools Manuf* 43:1383–1390. [https://doi.org/10.1016/S0890-6955\(03\)00130-5](https://doi.org/10.1016/S0890-6955(03)00130-5)
18. Soundararajan V, Atharifar H, Kovacevic R (2006) Monitoring and processing the acoustic emission signals from the friction-stir-welding process. *Proc Inst Mech Eng B J Eng Manuf* 220:1673–1685. <https://doi.org/10.1243/09544054JEM586>
19. Roy RB, Ghosh A, Bhattacharyya S, Mahto RP, Kumari K, Pal SK, Pal S (2018) Weld defect identification in friction stir welding through optimized wavelet transformation of signals and validation through X-ray micro-CT scan. *Int J Adv Manuf Technol* 99:623–633. <https://doi.org/10.1007/s00170-018-2519-3>
20. Fleming P, Lammlein D, Wilkes D et al (2008) In-process gap detection in friction stir welding 1:62–67. <https://doi.org/10.1108/02602280810850044>
21. Bhat NN, Kumari K, Dutta S, Pal SK, Pal S (2015) Friction stir weld classification by applying wavelet analysis and support vector machine on weld surface images. *J Manuf Process* 20:274–281. <https://doi.org/10.1016/j.jmapro.2015.07.002>
22. Fernández JB, Roca AS, Fals HC, Macías EJ, Partel MP (2012) Application of vibroacoustic signals to evaluate tools profile changes in friction stir welding on AA 1050 H24 alloy. *Sci Technol Weld Join* 1718:501–510. <https://doi.org/10.1179/1362171812Y.0000000040>
23. Gibson BT, Lammlein DH, Prater TJ, Longhurst WR, Cox CD, Ballun MC, Dharmaraj KJ, Cook GE, Strauss AM (2014) Friction stir welding: process, automation, and control. *J Manuf Process* 16:56–73. <https://doi.org/10.1016/j.jmapro.2013.04.002>
24. Krishnaveni V, Jayaraman S, Malmurugan N, Kandasamy A, Ramadoss D (2004) Non adaptive thresholding methods for correcting ocular artifacts in EEG. *Academic Open Internet Journal* 13
25. Pollock, Geoffrey DS, Green RC, Nguyen T, eds. (1999) *Handbook of time series analysis, signal processing, and dynamics*. Elsevier
26. Li CJ (2006) Signal processing in manufacturing monitoring. *Cond Monit Control Intell Manuf SE* 10:245–265. https://doi.org/10.1007/1-84628-269-1_10
27. Stéphane M (1999) *A wavelet tour of signal processing*. Elsevier
28. Gao RX, Yan R (2011) Wavelets: theory and applications for manufacturing. *Wavelets Theory Appl Manuf*:1–224. <https://doi.org/10.1007/978-1-4419-1545-0>
29. Oppenheim, Alan V (1978) *Applications of digital signal processing*, ph
30. Mishra D, Gupta A, Raj P, Kumar A, Anwer S, Pal SK, Chakravarty D, Pal S, Chakravarty T, Pal A, Misra P, Misra S (2020) Real time monitoring and control of friction stir welding process using multiple sensors. *CIRP J Manuf Sci Technol* 30:1–11. <https://doi.org/10.1016/j.cirpj.2020.03.004>
31. MEEN, RS, Sharma A (2014) Comparison and Analysis of Orthogonal and Biorthogonal Wavelets for ECG Compression. *International Journal of Research in Engineering and Technology* 3, no. 3: 242–247
32. Messer SR, Agzarian J, Abbott D (2001) Optimal wavelet denoising for phonocardiograms. *Microelectron J* 32:931–941. [https://doi.org/10.1016/S0026-2692\(01\)00095-7](https://doi.org/10.1016/S0026-2692(01)00095-7)
33. Ishan S, Banerjee S, Chattopadhyay T, Pal A, Garain U (2018) Systems and methods for obtaining optimal mother wavelets for facilitating machine learning tasks, US Patent App. 16:179–771
34. Ruqiang Y (2007) Base wavelet selection criteria for non-stationary vibration analysis in bearing health diagnosis. University of Massachusetts Amherst
35. Banerjee S, Chattopadhyay T, Pal A, Garain U (2018) Automation of feature engineering for IoT analytics. *ACM SIGBED Rev* 15: 24–30. <https://doi.org/10.1145/3231535.3231538>
36. Banerjee, Snehasis, Chattopadhyay T, Biswas S, Banerjee R, Choudhury AD, Pal A, Garain U (2016) Towards wide learning: Experiments in healthcare. arXiv preprint arXiv:1612.05730

Publisher's note Springer Nature remains neutral with regard to jurisdictional claims in published maps and institutional affiliations.